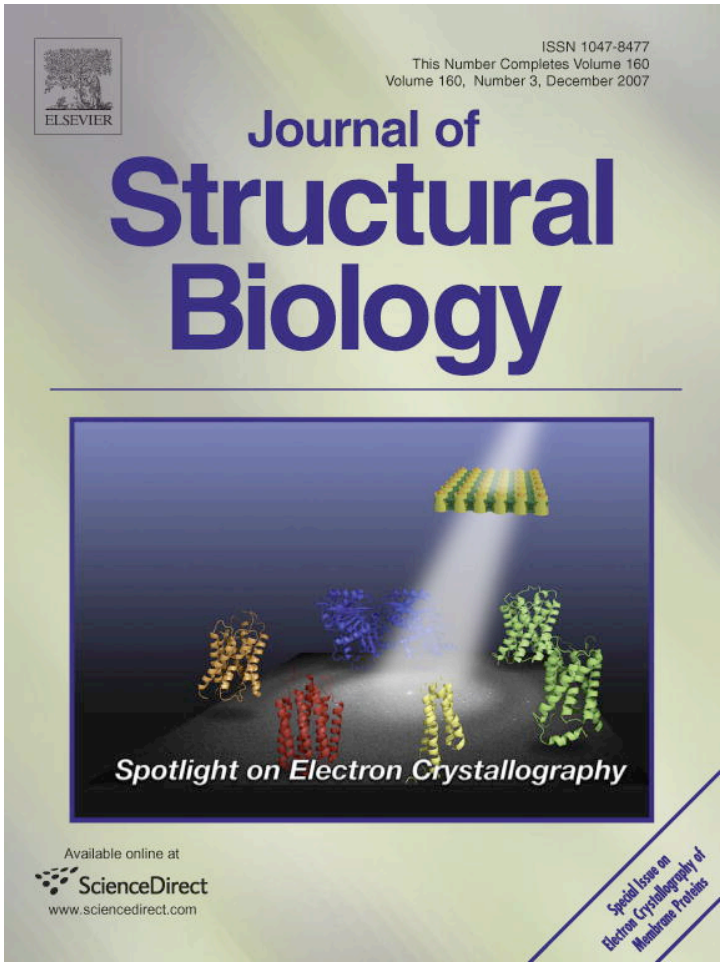

Available online at www.sciencedirect.com
ScienceDirect
Journal of Structural Biology 160 (2007) 295–304
Journal of Structural Biology
www.elsevier.com/locate/yjsbi

A high-throughput strategy to screen 2D crystallization trials of membrane proteins

Martin Vink [a], KD Derr [a], James Love [a,b], David L. Stokes [a,c], Iban Ubarretxena-Belandia [d,*]

[a] *The New York Structural Biology Center, 89 Convent Avenue, New York, NY 10027, USA*
[b] *New York Consortium on Membrane Protein Structure, 89 Convent Avenue, New York, NY 10027, USA*
[c] *Skirball Institute of Biomolecular Medicine and Department of Cell Biology, New York University School of Medicine, 540 First Avenue, New York, NY 10016, USA*
[d] *Department of Structural and Chemical Biology, Mount Sinai School of Medicine, 1425 Madison Avenue, New York, NY 10029, USA*

Received 2 May 2007; received in revised form 6 September 2007; accepted 7 September 2007
Available online 14 September 2007

Abstract

Electron microscopy of two-dimensional (2D) crystals has demonstrated potential for structure determination of membrane proteins. Technical limitations in large-scale crystallization screens have, however, prevented a major breakthrough in the routine application of this technology. Dialysis is generally used for detergent removal and reconstitution of the protein into a lipid bilayer, and devices for testing numerous conditions in parallel are not readily available. Furthermore, the small size of resulting 2D crystals requires electron microscopy to evaluate the results and automation of the necessary steps is essential to achieve a reasonable throughput. We have designed a crystallization block, using standard microplate dimensions, by which 96 unique samples can be dialyzed simultaneously against 96 different buffers and have demonstrated that the rate of detergent dialysis is comparable to those obtained with conventional dialysis devices. A liquid-handling robot was employed to set up 2D crystallization trials with the membrane proteins CopA from *Archaeoglobus fulgidus* and light-harvesting complex II (LH2) from *Rhodobacter sphaeroides*. For CopA, 1 week of dialysis yielded tubular crystals and, for LH2, large and well-ordered vesicular 2D crystals were obtained after 24 h, illustrating the feasibility of this approach. Combined with a high-throughput procedure for preparation of EM-grids and automation of the subsequent negative staining step, the crystallization block offers a novel pipeline that promises to speed up large-scale screening of 2D crystallization and to increase the likelihood of producing well-ordered crystals for analysis by electron crystallography.

Keywords: Two-dimensional (2D) crystals; Membrane proteins; Electron crystallography; High-throughput screening; Membrane protein reconstitution; Negative staining; 96-Well format; Crystallization block; Dialysis block

1. Introduction

Integral membrane proteins (IMPs)[1] comprise approximately 30% of the genes encoded in eubacterial, archaebacterial and eukaryotic genomes (Stevens and Arkin, 2000; Wallin and von Heijne, 1998), and play essential roles in cellular signaling and metabolism as receptors, enzymes, channels, transporters and structural proteins. IMPs are also pivotal in medicine and constitute the target of over 50% of current therapeutic drugs (Drews, 2000; Imming et al.,

* Corresponding author. Fax: +1 212 849 2456.
E-mail address: Iban.Ubarretxena@mssm.edu (I. Ubarretxena-Belandia).

[1] *Abbreviations used:* IMP, integral membrane protein; LPR, lipid-to-protein ratio; DDM, *n*-dodecyl-β-D-maltopyranoside; C12E8, polyoxyethylene(8)dodecyl ether; OG, *n*-octyl-β-D-glucopyranoside; LDAO, *n*-dodecyl-*N*,*N*-dimethylamine-*N*-oxide; DOPC, dioleoyl phosphatidylcholine; CMC, critical micelle concentration; LH2, light-harvesting complex II; EM, electron microscopy.

1047-8477/$ - see front matter © 2007 Elsevier Inc. All rights reserved.
doi:10.1016/j.jsb.2007.09.003

2006). Despite the relevance of membrane proteins to cell biology and to therapeutic medicine, to date only ~125 unique membrane protein structures have been deposited in the protein data bank (http://blanco.biomol.uci.edu/Membrane_Proteins_xtal.html). One reason for this huge knowledge-gap is that the prevalent protein structure determination methods, X-ray crystallography and NMR spectroscopy, suffer from technical limitations when it comes to IMPs. Unlike the soluble proteins routinely studied by these techniques, IMPs are embedded in the hydrophobic environment of the lipid bilayer and their amphiphilic nature hinders our ability to study them. Specifically, the main hurdles hampering membrane protein structure determination are: (i) problems in the routine over-expression of IMPs with native tertiary and quaternary structure; (ii) the loss of biological activity when IMPs are extracted from their native membrane environment with detergent; (iii) the large size of membrane protein/detergent complexes, which prevents the application of currently available solution NMR methods; and (iv) the difficulty in obtaining well-diffracting three-dimensional (3D) crystals for X-ray analysis. These problems are particularly severe for large, complex membrane proteins from eukaryotic origin.

An alternative approach to X-ray crystallography and NMR for the determination of membrane protein structure is electron crystallography of two-dimensional (2D) crystals (Henderson and Unwin, 1975). Indeed, this methodology has yielded atomic structures in the case of bacteriorhodopsin (Henderson et al., 1990), plant light-harvesting complex (Kühlbrandt et al., 1994), human red cell aquaporin-1 (Murata et al., 2000), eye lens aquaporin-0 (Gonen et al., 2005), rat aquaporin-4 (Hiroaki et al., 2006), glutathione transferase (Holm et al., 2006) and acetylcholine receptor (Unwin, 2005). The 3D structure of approximately 20 other unique membrane proteins have been determined to medium-resolution (5–8 Å), and continuing efforts are expected to produce atomic models in the near future (e.g. Hirai et al., 2002; Kukulski et al., 2005; Ubarretxena-Belandia et al., 2003). Electron crystallography is particularly well suited for IMPs that have a natural propensity to form 2D crystals within their native membranes. Unfortunately, these so-called "in situ" 2D crystals are quite rare and have only been found in special cases, e.g. when the concentration of the protein within the native membrane is high enough. Notable examples are bacteriorhodopsin from *Halobacterium halobium* (Henderson and Unwin, 1975) and Ca^{2+}-ATPase from mammalian sarcoplasmic reticulum (Dux and Martonosi, 1983; Xu et al., 2002) More generally, 2D crystals have been grown by reconstitution of purified, detergent-solubilized IMPs into lipid bilayers under defined conditions (for reviews see Jap et al., 1992; Kühlbrandt, 1992; Mosser, 2001). Reconstitution involves the controlled removal of detergent, either by dialysis (Kühlbrandt, 1992), controlled dilution (Remigy et al., 2003), adsorption onto a hydrophobic resin (Rigaud et al., 1997) or complexation to cyclodextrins (Signorell et al., 2006) in presence of a defined lipid-to-protein ratio (LPR). By achieving high density of a single protein species constrained to a 2D lipid bilayer, formation of a regular array—or 2D crystal—within this bilayer becomes relatively favorable.

2D crystallization of IMPs offers distinct advantages. Generally speaking, 2D crystallization can be performed at approximately 10-fold lower protein concentrations (0.4–1 mg/ml), than the concentrations required for 3D crystallization or for NMR data collection. Thus, only a small amount of material is required, an important consideration for IMPs with low expression levels, and sample aggregation that is common at high concentration of IMPs can be avoided. Moreover, 2D crystals provide a natural lipidic environment that is more likely to preserve the native conformation of the protein. Still, obtaining 2D crystals with the size and crystalline order required for structure determination by electron microscopy (EM) remains a challenge.

Identifying conditions for producing well-ordered crystals represents a significant bottleneck for any form of crystallography. Because these conditions are determined empirically there is a need for comprehensive screening. Indeed, rapid screening for 3D crystallization conditions has been critical in the recent explosion of X-ray crystallography, where a shotgun approach involving a large number of variables is generally required to produce crystals that diffract to high-resolution (Rees, 2001). Such rapid screening has been facilitated by the use of liquid handling robots to set up 24- or 96-well trays for vapor diffusion that can be rapidly screened by optical microscopy. In contrast, set up of dialysis trials for 2D crystallization has been neither fast nor automated. Furthermore, the small size of resulting 2D crystals (1–10 μm diameter and 5–10 nm thickness) requires electron microscopy to evaluate the results. In particular, each trial condition must be transferred to an EM grid, stained and inserted through an airlock into an electron microscope in a holder that typically holds just one grid at a time.

For this report, we have developed strategies for automating the screening of 2D crystallization of membrane proteins. We have designed a 96-well block for parallel dialysis trials, and employed a liquid-handling robot, both for setting up these trials, and for staining the EM specimens required for evaluating the screen. Two IMPs were used to evaluate the performance of the 96-well crystallization block and the quality of the staining procedure, namely CopA from *Archaeoglobus fulgidus* and light-harvesting complex II (LH2) from *Rhodobacter sphaeroides.* We also describe two alternatives for automated imaging of these samples within the electron microscope.

2. Materials and methods

2.1. Chemicals

The chemicals DDM (*n*-dodecyl-β-D-maltopyranoside), C12E8 (polyoxyethylene(8)dodecyl ether), OG (*n*-octyl-β-

D-glucopyranoside), LDAO (*n*-dodecyl-*N,N*-dimethylamine-*N*-oxide), and DOPC (dioleoyl phosphatidylcholine) were of the highest commercially available grade and were purchased from Anatrace (DDM, LDAO, OG), Nikkol (C12E8) and Avanti Polar Lipids (DOPC).

2.2. Quantification of detergent removal

The rate of detergent removal obtained with the 96-well crystallization block was determined by measuring the rate of transfer of the detergents OG (critical micelle concentration (CMC) = 5.3 mg/ml) and DDM (CMC = 0.087 mg/ml) from the sample well into the buffer chamber at room temperature. To start, 53 µl aliquots of 5 mg/ml OG or 1 mg/ml DDM were added to the sample wells and 1 ml of water was applied to each buffer chamber. In the case of OG, 50 µl aliquots were removed from the buffer chamber at defined time intervals, with each chamber providing only a single time point. A total of 11 time points were measured, each in triplicate, meaning that 33 total sample chambers provided samples for quantification. No buffer exchanges were carried out and we simply monitored the appearance of OG in the buffer chamber. In contrast, buffer exchanges were necessary for DDM. In this case, the entire contents of the buffer chamber was removed at each time point and replaced with a fresh supply of water. In both cases, the concentration of detergent in the buffer chamber was quantified using a colorimetric assay (Urbani and Warne, 2005). For OG, 50 µl aliquots from the chamber buffer contained enough detergent for reliable quantification. For DDM, the entire 1 ml fraction from the buffer chamber had to be concentrated by lyophilization before quantification.

2.3. Preparation of samples and set up of 2D crystallizations

Recombinant, purified CopA from the thermophilic bacterium *A. fulgidus* was a generous gift of Dr. C. Wu (Skirball Institute of Biomolecular Medicine, New York University, USA). This DDM-solubilized membrane protein was mixed with a stock solution of DOPC (2 mg/ml DOPC in 3.5 mg/ml C12E8) to a final protein concentration of 0.5 mg/ml and LPR of 0.5 and 0.6. Aliquots of 53 µl were transferred to the sample wells of the crystallization block and dialyzed at 20 °C against buffer. The dialysis buffer was exchanged twice during the first day and once daily thereafter. Following a defined period of dialysis, the dialysis buffer was removed and each sample was recovered by puncturing the dialysis membrane with the tip of a pipette. A small aliquot of each sample was then used for negative staining.

Purified LH2 from the purple bacterium *R. sphaeroides* solubilized in LDAO was a generous gift from Drs. J.A. Timney and C.N. Hunter (Department of Molecular Biology and Biotechnology, Sheffield University, UK). The conditions used for LH2 crystallization have been reported previously (Walz et al., 1998). The protein was mixed with a stock solution of DOPC (4 mg/ml DOPC in 8 mg/ml OG) to produce a final protein concentration of 0.5 mg/ml and LPRs of 0.2, 0.5, 0.8 and 2.0. Aliquots of 53 µl were transferred to the sample wells of the crystallization block and dialyzed against a buffer consisting of 10 mM Hepes pH 7.5, 100 mM NaCl, 0.5 mM NaN_3 for 24 h at 30 °C. Samples were recovered in the same way as CopA.

For dialysis of both proteins, a flat dialysis membrane (MWCO: 12,000 Da, Spectrum Laboratories Inc.) was boiled in 5 mM EDTA at pH 8.0, cut to match the size of the crystallization block and placed in between the two halves of the block after loading the sample wells with the protein–lipid mixture. Dialysis buffer was added to the top chamber after securing the two halves of the block together.

2.4. EM grid preparation, automated negative staining and imaging

A crystallization dish (10 cm diameter) was completely filled with tap water and the surface was swept clean with a glass pipette. Twenty-five microliters of an amyl acetate solution containing 1% nitrocellulose were dispensed onto the water, and evaporation of the solvent produced a thin film of nitrocellulose that covered the entire surface. Cu EM grids (300 mesh) were then placed individually onto this film with a pair of tweezers. The grids were collected by blotting a piece of clean print-free newspaper onto the surface of the dish and carefully lifting up the entire batch of grids. The newspaper and the grids were left to dry with the nitrocellulose film facing upwards. Carbon coating and glow discharging were carried out using a vacuum evaporator (AUTO 306, BOC Edwards, Crawley UK). The newspaper and attached grids were placed in the vacuum evaporator and were coated with a continuous carbon film under high vacuum. A 1 mm diameter carbon thread was used for evaporation of a reproducible thickness of carbon (~7 nm). Immediately thereafter, the grids were glow discharged for 30 s in air. Using this procedure a large batch of several hundred grids could be prepared simultaneously.

The automated negative staining was carried out as follows. Using a paintbrush each of the small platforms on the staining block was coated with a thin layer of grid-stick glue (Electron Microscopy Sciences, Hatfield PA) and the staining block was thereafter baked for 10 min in an oven at 150 °C. This glue provides a sticky surface that can be used repeatedly for retaining the grids on the surface of the block during the staining procedure; when the glue wears off it can easily be re-applied in the same way. Freshly prepared carbon coated grids were manually placed onto the grid-platforms of the staining block with a pair of tweezers and the block was placed in the Biomek FX liquid-handling robot (Beckmann-Coulter, Fullerton CA) that was programmed to carry out the following staining protocol on all the grids in parallel: 2 µl of each crystallization trial was applied onto the carbon grid for 30 s followed by 5 µl of stain (0.5% uranyl acetate in water).

After removing 5 μl of this solution, another 5 μl of stain was applied onto the grid followed by an immediate removal of 5 μl of solution. This procedure was repeated one more time and in the final aspiration step all remaining liquid was removed from the grids, which were then allowed to dry. Samples were examined in a JEM-1230 transmission electron microscope (JEOL, Tokyo Japan) at an accelerating voltage of 80 keV and images were recorded on a 1K × 1K CCD camera (Erlangshen, Gatan Inc., Pleasanton CA).

3. Results and discussion

3.1. Design and construction of a 96-well 2D crystallization block

2D crystallization involves the removal of detergent in the presence of lipid in order to reconstitute a given IMP into a lipid bilayer under conditions that are amenable to the formation of a 2D crystal. Dialysis is the most common method for detergent removal and has generally involved laborious procedures involving the use of dialysis bags, cassettes or buttons (Kühlbrandt, 1992), which limit the number of parallel conditions that an investigator can manage. Several devices for parallel dialysis have been described for 2D crystal screening but, in general, these provide a limited number of chambers for testing different conditions and do not interface well with liquid-handling robotic systems operating on a 96-well microtiter format (Engel et al., 1998; Jap et al., 1992; Paul et al., 1992). 96-well dialysis plates are also commercially available, but they are severely limited since all 96 different protein samples have to be dialyzed against a common buffer (e.g. the 96-Well Dispo-Dialyser from The Nest Group). Ideally, a 96-well crystallization device should offer the possibility to dialyze 96 different crystallization trials against 96 unique dialysis buffers. Such a device will offer enhanced flexibility to screen a given protein solution, with a defined lipid type and LPR, against a range of dialysis buffers having various pH's, ionic strengths, inhibitors or substrate analogs.

We have therefore designed a crystallization block using the geometry and dimensions of the standard 96-well format to allow for automation of crystallization trials. This block can be cheaply reproduced and allows for simultaneous dialysis against 96 different buffers (Fig. 1). The block consists of a lower part that accommodates the dialysate wells and an upper part containing the chambers for the dialysis buffer. The dialysis membrane is placed in the space in between the upper and lower parts. SBS standards for micro-plate dimensions were used for the outer dimensions (8.55 × 12.8 cm) of the block and for the spacing of the wells (9 mm center-to-center, for a full set of standard dimensions, refer to http://www.sbsonline.org/msdc/). To allow for visual inspection during the dialysis process, the block was made out of transparent acrylic plastic (Fig. 1c).

The sample wells were designed to optimize the contact area between dialysate and dialysis buffer and thus maximize the rate of detergent removal. These wells were therefore made 5 mm in diameter but only 3 mm deep, with a 50 μl capacity, and with a conical bottom to facilitate sample removal after completion of dialysis (Fig. 1b). The chamber for the dialysis buffer in the upper part of the crystallization block has a 6 mm diameter and 37 mm height with a capacity of 1.1 ml. Each exchange of dialysis buffer thus dilutes the sample >20-fold. The pipette tips must ultimately puncture the dialysis membrane to retrieve the dialysate. Therefore, the standard pipette tip length used by the Biomek FX liquid handler, employed for automation of the dialysis process, constrains the height of the buffer chambers, and hence their capacity.

To assemble the crystallization block, samples were loaded into the dialysate wells, the upper part was inverted and the wet dialysis membrane was placed on top. Air bubbles and folds were carefully removed from the dialysis membrane and the upper block was placed on top of the lower block using the metal guide pins located in the opposite corners of the lower block (diameter 4.5 mm). These guide pins ensure that the block faces remain parallel during the assembly. After establishing contact, the two parts were secured with six stainless steel screws on the long side of the block (Fig. 1a and c). Initially these screws tapped directly into the acrylic plastic on the lower part of the block, but we found that tightening the screws caused the acrylic to crack. To distribute the force more evenly, the upper edge of the block was cut away and replaced by an aluminum bar (6 × 6 × 100 mm) with holes to accommodate the screws. Likewise, the edge of the lower block was replaced with an aluminum bar of the same dimensions as the upper bar with threaded receptacles to receive the screws (Fig. 1a and c). The aluminum bars were glued onto the block by the use of 5-min epoxy.

Initially, we did not use the silicone gaskets shown in Fig. 1 and despite parallel and level surfaces on both the upper and lower faces of the block and care in sealing the blocks, leakage between adjoining wells was substantial. When grease was applied onto the upper and lower block faces, leakage was significantly reduced. However, the grease had a tendency to spread into the wells and partly cover the dialysis interface, thus diminishing the rate of dialysis. Furthermore, the use of grease made the parts slippery and difficult to handle. Next, we applied a small ring of silicone caulk around the circumference of each well—both upper and lower block faces—and allowed to cure. The compressibility and inertness of the silicone produced an ideal seal and almost no leakage was observed between the wells. However, fresh silicone rings had to be reapplied for each new dialysis trial and this process was time-consuming. In our final design, a soft silicone sheet (McMaster-Carr, #9010K811) has been fashioned into a gasket on either side of the dialysis sheet. Having a thickness of only 0.8 mm, this sheet is very flexible yet robust and possesses both the compressibility and inertness of the silicone caulk. The silicone sheet was cut to the size of the crystallization block and holes corresponding to

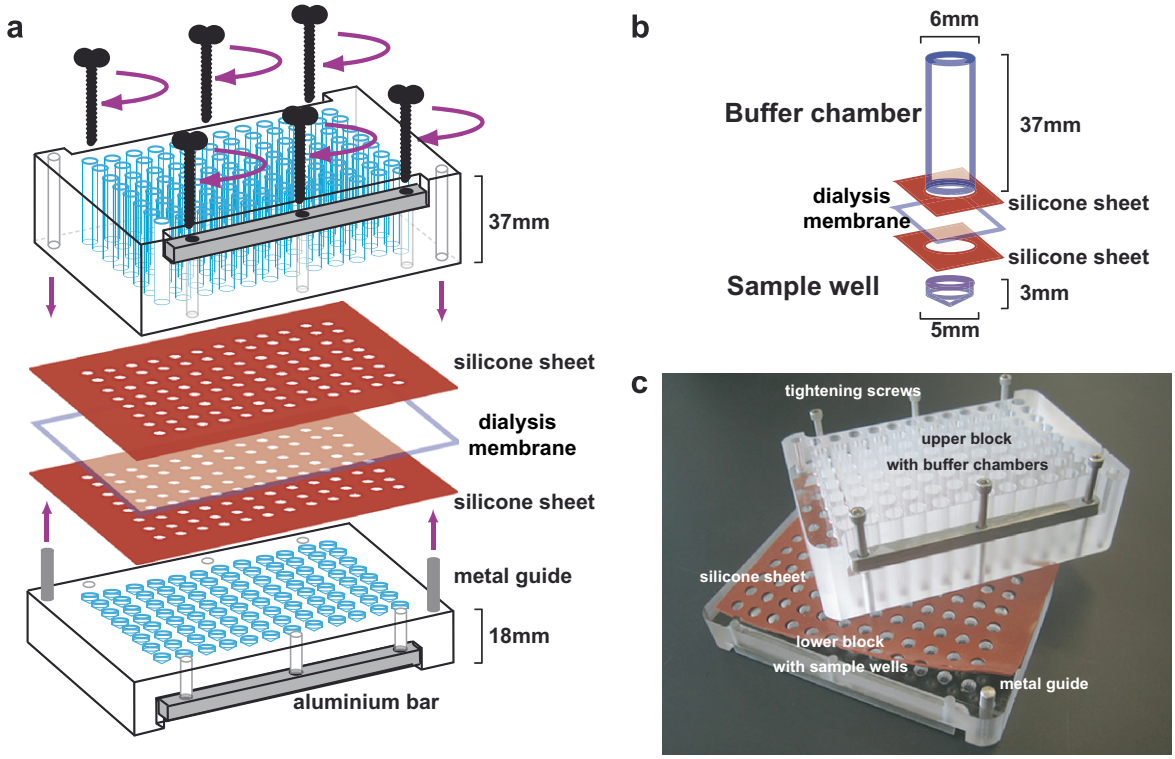

Fig. 1. The 96-well 2D crystallization block. (a) A schematic representation of the crystallization block is shown. The metal guides are positioned diagonally in two of the corners of the lower block to aid the assembly of the upper and lower block parts, and the six screws are used to keep the block tightly sealed after assembly. Note that the silicone sheets are necessary both above and below the dialysis membrane to prevent leakage. (b) View of an individual dialysis unit illustrating dimensions of the sample well and the buffer chamber. (c) Photo of the crystallization block prior to assembly in which various parts are shown. The dialysis membrane and one of the silicone sheets are omitted for clarity.

the buffer chambers and/or sample wells were punched in the sheet using a custom-made cork-borer with the upper block as a template for the positions of the holes. The silicone is intrinsically sticky and, once centered over the holes, remains tightly stuck to the surfaces of the crystallization block. Furthermore, the silicone is easy to clean and reusable. Most importantly, leakage between adjoining wells was undetectable when the silicone sheets were used on both sides of the dialysis membrane (Fig. 1).

During assembly of the crystallization block it was discovered that small air bubbles formed in the sample wells in the contact area between the chambers and the dialysis membrane. However, optimizing the volume in the sample well minimized these air bubbles. With the added thickness of the silicone gasket, the optimal volume of loaded sample was 53 µl. Undoubtedly, air bubbles hamper dialysis since they reduce the contact area between sample and buffer, however, due to the miniscule size of the bubbles under optimal loading conditions, their effect on the rate of dialysis is probably very limited.

The Biomek FX liquid-handling robot allows for automation of crystallization trials using the crystallization block. This robot loads protein samples in the dialysis wells and, after assembly of the block, carries out buffer addition, exchange and removal. At the end of the crystallization period, the robot retrieves the dialysate by punching a hole through the dialysis membrane transferring the samples either to another microtiter plate for storage or directly onto EM grids for staining. Moreover, in between the buffer exchange steps, the robot can be used to mix or to exchange the dialysis buffer, thus minimizing gradients from building up and slowing down the rate of dialysis.

3.2. Design and implementation of a negative staining procedure in a 96-well format

A high-throughput workflow for the screening of 2D crystals includes not only dialysis, but also procedures for preparing EM grids and for staining samples in a reproducible and parallelized way. Using a thin plastic layer as a support for carbon film is a common strategy for preparing robust carbon substrates for negative staining, and can be faster than floating evaporated carbon off a mica surface (Harris, 1997). Preparation of a batch of grids with attached plastic can be accomplished within minutes by pipetting nitrocellulose dissolved in amyl acetate onto a clean water surface, and allowing the amyl acetate to evaporate. The resulting plastic film provides a resilient substrate for supporting Cu EM grids on the water surface, which can then be picked up *tout ensemble* with a piece of newspaper. Since the ensuing carbon evaporation and glow discharge are performed using the same vacuum evaporator operated in different modes, the throughput for carbon-coated grid production is high.

Unlike detergent removal by dialysis, negative staining of samples is not innately time consuming. Nevertheless, negative staining requires multiple steps of pipetting and blotting and thus constitutes a significant bottleneck in a high-throughput screen. However, these steps are amenable to automation with a liquid-handling robot. A grid-staining plate (Fig. 2) made up from 96 cubical platforms, cut from aluminum and spaced according to standard microplate dimensions (http://www.sbsonline.org/msdc/) was developed. EM grids were placed atop these cubical platforms, whose 2 mm dimension was slightly smaller than the 3 mm diameter of a conventional EM grid. These platforms allow easy placement of grids with forceps and also minimize the wicking of solution to the backside of the grids. The robot was then used to apply specimens and to stain the grids (see Section 2). We note that although we used forceps, a suction pipette (Vacuum Pick Up System, Electron Microscopy Sciences) for handling the grids represents a good alternative that should be considered and that could lend itself to further automation with a robotic arm.

Early trials with the grid-staining plate focused on the task of attaching the grids onto the platform. If the interaction was too strong the grids became deformed or tore when trying to remove them after staining. On the other hand without an adhesive, the grids were displaced or even removed by capillary action during the pipetting steps needed in the staining protocol. Glycerol and vacuum grease (Fomblin) were evaluated as adhesives, but their greasy texture made the grids difficult to handle. A solution of 2% sorbitol in distilled water performed well as an adhesive and did not affect carbon film quality. For adhesion, a small amount of sorbitol solution was spread onto each platform using a paintbrush, grids were placed on the platforms and the solvent was allowed to evaporate, thus attaching the individual grids to their staining platforms. However, a fresh application of sorbitol was required for every round of staining and the evaporation step took a considerable amount of time, thus detracting from our goal of high-throughput. A more effective alternative is to apply a thin layer of Grid-Stick Glue (Electron Microscopy Sciences), which has been specifically developed to act as temporary adhesive for EM grids during negative staining. Like the sorbitol solution, this glue was applied to the platforms with a paintbrush and the staining plate was then baked at 150 °C for 10 min according to the manufacturer instructions. The glue retained its adhesiveness for several rounds of negative staining, and when it wore off, it was easily replenished by administering a new layer of glue. It should be noted that our original staining block was made of plastic, which shrank slightly after baking and prompting us to switch to aluminum.

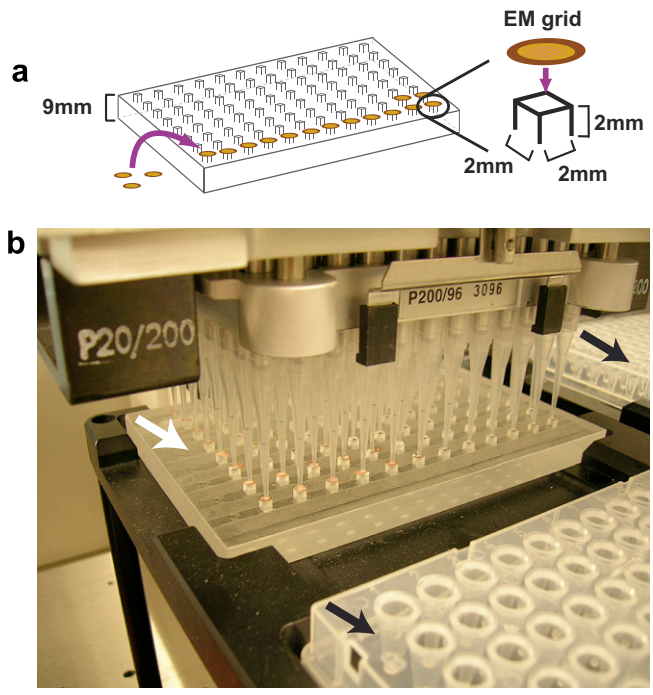

Fig. 2. The 96-grid staining block. (a) A diagram of the negative staining block displaying the cubical platforms supporting the grids during the staining process. The carbon-coated EM grids are attached onto the platform one-by-one using Grid Stick Glue as adhesive. (b) A close-up of the staining block (white arrow) during one of the pipetting steps by the Biomek FX liquid-handling robot. Microtiter trays holding samples and negative stain surround the block (black arrows).

After loading all the grids onto the staining platforms the grid-holder was transferred to the robot. The robot carried out sample application and staining with uranyl acetate on all grids in parallel (see Section 2). Results using this automated method for negative staining were comparable to manual methods (Figs. 4 and 5).

3.3. Rate of detergent removal

2D crystallization by detergent dialysis is intrinsically slow due to the fact that only detergent monomers, but not higher order micelles, can pass through a dialysis membrane. Thus, the chemical potential for detergent dialysis is limited by the CMC (Helenius et al., 1979). This limit is extreme for detergents with low CMC that are often used for membrane protein solubilization. Therefore, the efficiency of detergent removal is an important consideration for our 96-well crystallization block. We therefore measured the rate of dialysis for the high CMC detergent OG as well as for the low CMC detergent DDM at room temperature. Starting from an OG concentration equal to the CMC (5.3 mg/ml), approximately 50% of the detergent was removed from the sample well after 2.5 h and equilibrium between the two chambers was reached after approximately 24 h of dialysis (Fig. 3a). For OG, these measurements were carried out without exchanging the dialysis buffer and values plotted in Fig. 3a correspond to the concentration measured in the dialysis buffer, which had 20 times the volume of the sample.

In contrast, the rate of dialysis of DDM was significantly slower due to its very low CMC (0.087 mg/ml) relative to the concentration effective for membrane protein

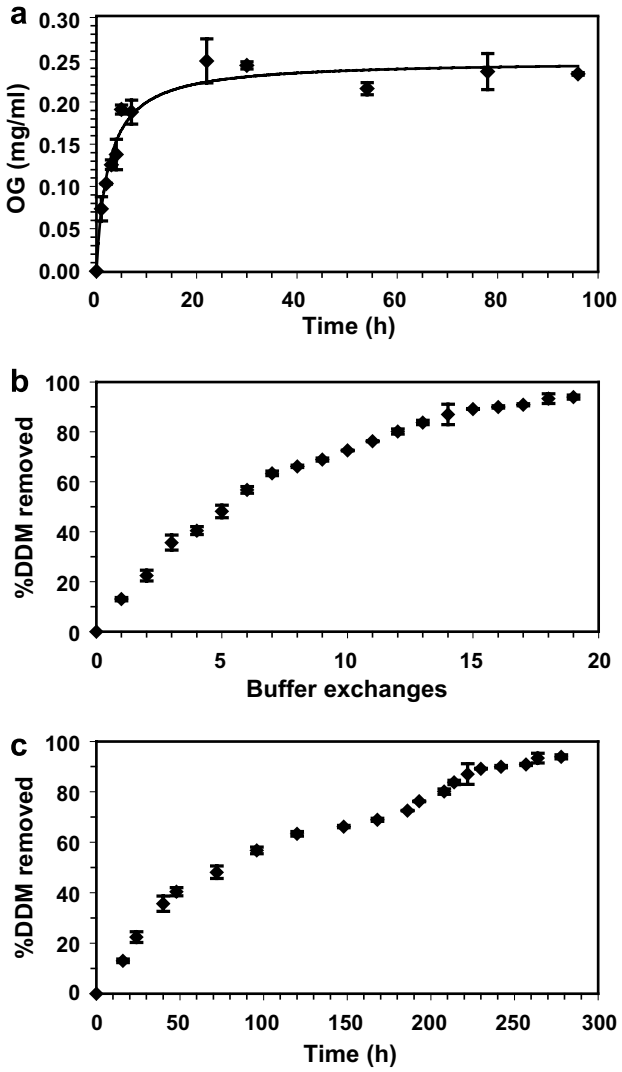

Fig. 3. Rate of detergent removal using the 96-well crystallization block. (a) The time-dependent increase in OG concentration in the buffer chamber illustrates the kinetics of OG dialysis. The data fits to a hyperbolic saturation curve and error bars indicate the standard deviation between three parallel samples. The initial concentration of OG in the sample well was 5 mg/ml and the final measured concentration in the buffer chamber was 0.24 mg/ml. Considering the 20-fold difference in volumes, these values indicate that equilibrium had been achieved after ~24 h. (b) DDM removal was plotted as function of buffer exchange. The rate of removal was linear for the first 7 exchanges, after which it leveled off slightly as the concentration in the sample well decreased. (c) The same data for DDM removal displayed in (b) is now plotted against time. This shows that the overall rate of DDM removal depends strongly on the frequency of buffer exchange. All detergent dialysis experiments were carried out at room temperature.

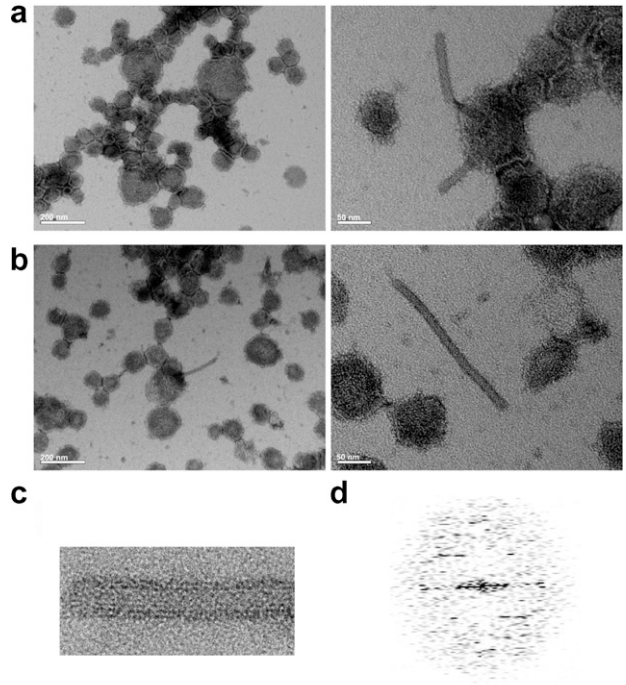

Fig. 4. Negative stain electron microscopy of CopA crystallization. (a) Dialysis performed at 20 °C for four days at an LPR of 0.6. Left, a medium-magnification image of negatively stained CopA after 4 days of dialysis at 20 °C illustrates that CopA has been reconstituted into proteoliposomes. Right, a high-magnification image of the same sample shows very thin, elongated, tubular crystals beginning to grow. (b) Dialysis performed at 20 °C for 1 week at an LPR of 0.6. (Left) In the medium-magnification image, elongated tubular crystals were found interspersed among proteoliposomes. (Right) A high magnification image of one of the CopA tubular crystals. The scale bar represents 200 nm in the medium-magnification left panel and 50 nm in the right panel. (c) A close-up of one of the CopA crystals where the helical crystalline lattice can be seen. (d) The calculated diffraction pattern (without unbending) from the area displayed in C. Although the pattern from helical crystals is expected to have mirror symmetry, uneven staining is likely responsible for the non-symmetric pattern seen in these sample.

solubilization (1 mg/ml). To speed up dialysis of DDM, we systematically refreshed the dialysis buffer. The corresponding plots (Fig. 3b and c) do not, therefore, reflect an equilibrium and are strongly influenced by the frequency of the buffer exchange. Note that Fig. 3b plots DDM removal as a function of buffer exchange, whereas Fig. 3c plots the same data as a function of time. After the first buffer exchange (20 h), ~10% of the total DDM was removed, reflecting virtually complete equilibration of the CMC across the dialysis membrane. This situation applied to the first 7 buffer exchanges, when the concentration gradient across the membrane was at its highest (Fig. 3b). Thereafter, the removal rate decreased, such that ~20 buffer exchanges were required to fully deplete DDM from the sample well (Fig. 3b). The ability to completely remove DDM over 12–13 days compares favorably with conventional dialysis devices, emphasizing the suitability of our 96-well crystallization block for detergent removal.

The dialysis rate of DDM was strongly dependent on the frequency of buffer exchange. The time interval between buffer exchanges plotted in Fig. 3b and c varied between 5 h and 24 h, both of which appeared to offer sufficient time to equilibrate the concentration of DDM across the dialysis membrane. Thus, after 190 h of dialysis, the curve in Fig. 3c steepens as the rate of buffer exchange is increased. This implies that it is possible to control the rate of dialysis of a low CMC detergent via the frequency of buffer exchanges, as long as the interval between two con-

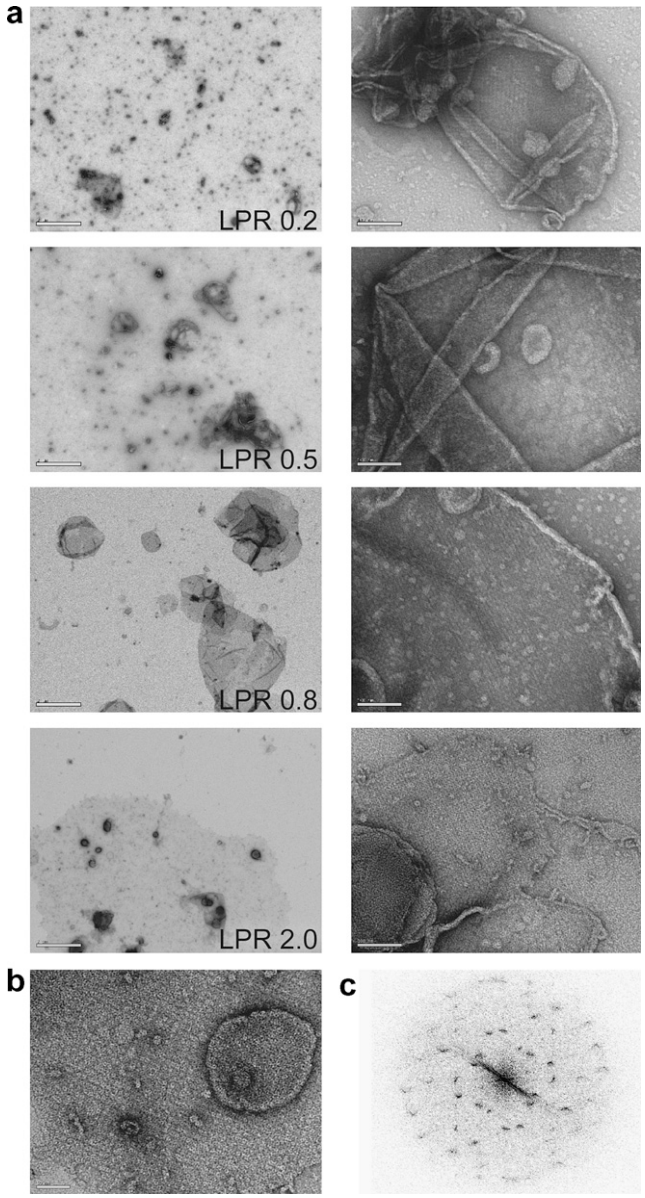

Fig. 5. Negative stain electron microscopy of 2D crystals of LH2. (a) Negatively stained micrographs of vesicular 2D crystals of LH2 formed after a 24 h dialysis at 30 °C. The left panel shows the crystals in low-magnification mode with the LPR indicated. Note the differences in crystal size observed between the different LPRs. The right panel shows a medium-magnification of the crystals from each of the LPRs displayed in the left panel. 2D crystal lattices were found at all LPRs. (b) A high-magnification image of one of the crystals shows the square lattice formed by LH2 complexes. (c) The calculated diffraction pattern (without unbending) from the LH2 crystal reveals two sets of diffraction spots originating from the proximal and distal 2D lattices of the collapsed vesicular crystal. The scale bars represent 2 μm, 100 nm and 50 nm for low-, medium- and high-magnification, respectively.

secutive changes is >5 h. Thus, a plausible strategy for 2D crystallization would be to rapidly deplete the bulk detergent at the start of dialysis with frequent buffer exchanges; once detergent levels reach the critical level for reconstituting a bilayer, intervals between buffer changes could be increased to allow sufficient time for crystallization.

3.4. 2D crystallization trials on CopA and LH2

To test the efficacy of our 96-well crystallization and grid staining devices, CopA from the thermophilic bacterium *A. fulgidus* and LH2 from the purple bacteria *R. sphaeroides* were used for exploratory 2D crystallization trials. For CopA, 2D crystallization has not yet been reported, whereas for LH2, crystallization conditions have been described previously (Walz et al., 1998). Since the main purpose of this report is to demonstrate the design and viability of the crystallization block and the automated staining procedure, we set up dialysis under a relatively narrow set of conditions designed as a proof of principle, and did not set up extensive crystallization screens necessary to optimize crystallization conditions for either of these two proteins.

CopA is an ATP-dependent Cu^+ pump that is responsible for the cellular export of Cu^+ from the thermophile *A. fulgidus*. It is a member of the P-type ATPase family, which also includes related Cu^+ pumps responsible for Wilson and Menkes diseases in humans (Sazinsky et al., 2006). CopA has eight transmembrane helices and has a molecular weight of 86 kDa. For crystallization trials, CopA was solubilized in 0.01% DDM and mixed with DOPC and C12E8 at a final protein concentration of 0.5 mg/ml with LPRs of 0.5 and 0.6 (final C12E8 concentration of 0.5 and 0.6 mg/ml). Both DDM and C12E8 are detergents with low CMCs that generally require dialysis periods of 1–2 weeks for 2D crystallization (Kühlbrandt, 1992; Mosser, 2001). Dialysis was performed at 20 °C and the dialysis buffer was exchanged twice the first day and daily thereafter. After four days, protein reconstitution into vesicular structures was evident in both LPRs (Fig. 4a left panel) and characteristic tubular structures started to appear in the sample with an LPR of 0.6 (Fig. 4a right panel). After an additional three days of dialysis at 20 °C, these tubular proteosomes had increased both in length and in abundance in the sample with an LPR of 0.6 (Fig. 4b) and could at this point be detected also in the sample with an LPR of 0.5 (not shown). At closer inspection, many of the tubes were found to contain crystalline lattices that displayed some diffraction (Fig. 4c and d). These results for CopA are comparable to those obtained using dialysis buttons (C. Wu and D.L. Stokes, unpublished results).

Next we employed the light-harvesting protein LH2 from the purple bacterium *R. sphaeroides*, to test the 96-well crystallization block using an IMP with well-established 2D crystallization conditions and a detergent with a higher CMC (Walz et al., 1998). LH2 is a heterodimer made up of two pigment binding subunits α and β, each approximately 5 kDa in weight and with a single transmembrane helix topology (Olsen et al., 1997). It constitutes the external, mobile antenna that surrounds the photosynthetic core reaction center/light-harvesting complex I and is present with variable stoichiometry depending on light conditions (Scheuring and Sturgis, 2005). The LH2 is organized into large ring-like complexes comprised of nine αβ

heterodimers, the structure of which was determined at 6 Å resolution by electron crystallography (Walz et al., 1998).

For screening the crystallization behavior of LH2, we chose to use a defined dialysis buffer that is known to produce 2D crystals and to explore the effect of LPR on crystal morphology. LH2 was purified in the detergent LDAO and mixed with DOPC dissolved in OG with a final protein concentration of 0.5 mg/ml and LPRs of 0.2, 0.5, 0.8 and 2.0. After incubation in the crystallization block for 24 h at 30 °C, specimens were harvested, stained and imaged in the electron microscope. In all conditions, vesicular crystals containing 2D ordered arrays could be observed. As expected, the crystals had different morphologies depending on the LPR (Fig. 5a): LPR of 0.2 produced only small 2D crystals and much aggregated protein, whereas LPR of 2.0 produced large lipid sheets with small areas containing 2D protein crystals. Crystals from intermediate LPRs had intermediate morphologies with an LPR of 0.8 producing an optimal combination of large 2D crystalline arrays with minimal protein aggregation. The original detergent-solubilized LH2 solution contained only solubilized proteins and was completely devoid of either protein aggregates, membrane sheets or 2D crystalline arrays (not shown). Calculated diffraction patterns from the LH2 arrays displayed two sets of diffraction spots originating from 2D square lattices on the proximal and distal sides of the collapsed vesicular crystal (Fig. 5c). These results are comparable to those previously reported using traditional dialysis methods (Walz et al., 1998). The reproducibility of 2D crystallization was tested by running these conditions in triplicate wells and by repeating the crystallization with the same protein batch on different days. In both cases, we observed the same effects of LPR on crystallization and consistently obtained 2D protein arrays. This outcome also indicates that the small air bubbles present at the dialysis membrane interface, despite variability in size and number, do not present any significant impediment to the dialysis process.

The shorter time period for crystallization of LH2 compared to CopA (24 h vs. 7 days) reflects the faster rate of detergent removal for the higher CMC detergents like OG compared to low CMC detergents like DDM and C12E8. The successful reconstitution and crystallization of both CopA and LH2 illustrates the suitability of our 96-well block for membrane protein 2D crystallization, both for low and high CMC detergents.

4. Conclusions

In this communication we have presented tools that we believe will facilitate the process of screening conditions for 2D crystallization. Experience in X-ray crystallography shows that a comprehensive screen over a wide range of conditions is imperative for increasing the applicability of any crystallographic technique, especially when the methods for structure determination, in this case electron crystallography, are well established. Experience shows that, if the crystals are suitable, electron crystallography is capable of achieving atomic resolution. Indeed, the 96-well format for dialysis and negative stain EM grid preparation provides a platform for testing a wide range of crystallization factors, including lipid composition, LPR, pH, and physiological ligands. Initially, this screen should be designed to sample a broad range of the multifactorial crystallization space. After identifying a specific number of positive ''hits'', a process of optimization is inevitable in order to obtain large, well-ordered crystals that will produce the highest resolution structure. This latter step of optimization would also benefit from the high-throughput strategy offered by our 96-well screening device but, given the ambiguities of crystallization, more conventional methods of dialysis or biobeads addition should also be considered. Results will certainly be case-specific, and considerably more experience will be required before arriving at any general conclusions.

One important aspect of the screening process that has not yet been mentioned is imaging of these crystallization trials in an efficient and rapid way. Loading of grids in and out of a microscope followed by imaging and evaluation, are all processes that require significant time and effort. There have been advances in automating these processes. Notably, a robot has been developed by Potter and colleagues at the National Resource for Automated Molecular Microscopy at Scripps that is able to pick up grids one-by-one and to load them into the microscope for imaging (Potter et al., 2004; Stagg et al., 2006). When combined with the Leginon software for automated imaging of EM grids (Potter et al., 1999; Suloway et al., 2005), this robot is able to work through samples in an unattended manner, presenting the researcher with a series of digital images for later evaluation. Alternatively, the laboratory of Dr. Subramaniam (National Cancer Institute of National Institutes of Health, Bethesda MD) has collaborated with a commercial vendor (Gatan Inc.) to develop a cartridge-based specimen holder that simultaneously holds 100 samples within the electron microscope (Lefman et al., 2007). This system also includes software for automated imaging. Although we have not used either system, we estimate that 20–30 min would be required to image each sample, so that imaging an entire 96-well screen will require 32–48 h. By combining our screening approach with recent efforts to increase the user-friendliness and to reduce the time required for image processing of 2D crystals (Gipson et al., 2007), we hope that electron crystallography will assume its rightful place as a viable and complementary alternative to X-ray crystallography and NMR spectroscopy in membrane protein structure determination.

Acknowledgments

We are indebted to Dr. C. Wu at the Skirball Institute of Biomolecular Medicine (New York, USA) for his generous gift of CopA and to Drs. J.A. Timney and C.N. Hunter at Sheffield University (Sheffield, UK) for their kind gift of LH2 complexes. We also wish to thank Mr. R. Hinchliffe

at the City College of New York (New York, USA) for help with manufacturing the crystallization block and the staining plate, and Dr. K. Mitra at the Wadsworth Center (Albany, USA) and Mr. J. Riley at the New York Structural Biology Center for help with their design. We are also grateful to Drs. A. Siebert and W. Rice at the New York Structural Biology Center for fruitful discussions. National Institutes of Health Grants U54 GM075026 to the New York Consortium on Membrane Protein Structure, R01 GM56960 and R01 GM081817 to DLS, and National Science Foundation Grant MCB-0546087 to IU-B supported this work.

References

Drews, J., 2000. Drug discovery: a historical perspective. Science 287, 1960–1964.

Dux, L., Martonosi, A., 1983. Two-dimensional arrays of proteins in sarcoplasmic reticulum and purified Ca2+ATPase vesicles treated with vanadate. J. Biol. Chem. 258, 2599–2603.

Engel, A., Holzenburg, A., Stauffer, K., Rosembusch, J., Aebi, U., 1998. Proceedings of the 46th Annual Meeting of the Electron Microscopical Society of America. San Francisco Press, San Francisco, pp. 152–153.

Gipson, B., Zeng, X., Zhang, Z.Y., Stahlberg, H., 2007. 2dx—user-friendly image processing for 2D crystals. J. Struct. Biol. 157, 64–72.

Gonen, T., Cheng, Y., Sliz, P., Hiroaki, Y., Fujiyoshi, Y., Harrison, S.C., Walz, T., 2005. Lipid-protein interactions in double-layered two-dimensional AQP0 crystals. Nature 438, 633–638.

Harris, J.R., 1997. Negative staining and cryoelectron microscopy BIOS scientific publishers.

Helenius, A., McCaslin, D.R., Fries, E., Tanford, C., 1979. Properties of detergents. Methods Enzymol. 56, 734–749.

Henderson, R., Unwin, P.N.T., 1975. Three-dimensional model of purple membrane obtained by electron microscopy. Nature 257, 28–32.

Henderson, R., Baldwin, J.M., Ceska, T.A., Zemlin, F., Beckmann, E., Downing, K.H., 1990. Model for the structure of bacteriorhodopsin based on high-resolution electron cryo-microscopy. J. Mol. Biol. 213, 899–929.

Hirai, T., Heymann, J.A., Shi, D., Sarker, R., Maloney, P.C., Subramaniam, S., 2002. Three-dimensional structure of a bacterial oxalate transporter. Nat. Struct. Biol. 9, 597–600.

Hiroaki, Y., Tani, K., Kamegawa, A., Gyobu, N., Nishikawa, K., Suzuki, H., Walz, T., Sasaki, S., Mitsuoka, K., Kimura, K., Mizoguchi, A., Fujiyoshi, Y., 2006. Implications of the aquaporin-4 structure on array formation and cell adhesion. J. Mol. Biol. 355, 628–639.

Holm, P.J., Bhakat, P., Jegerschold, C., Gyobu, N., Mitsuoka, K., Fujiyoshi, Y., Morgenstern, R., Hebert, H., 2006. Structural basis for detoxification and oxidative stress protection in membranes. J. Mol. Biol. 360, 934–945.

Imming, P., Sinning, C., Meyer, A., 2006. Drugs, their targets and the nature and number of drug targets. Nat. Rev. Drug Discov. 5, 821–834.

Jap, B.K., Zulauf, M., Scheybani, T., Hefti, A., Baumeister, W., Aebi, U., Engel, A., 1992. 2D crystallization: from art to science. Ultramicroscopy 46, 45–84.

Kühlbrandt, W., 1992. Two-dimensional crystallization of membrane proteins. Q. Rev. Biophys. 25, 1–49.

Kühlbrandt, W., Neng Wang, D., Fujiyoshi, Y., 1994. Atomic model of plant light-harvesting complex by electron crystallography. Nature 367, 614–621.

Kukulski, W., Schenk, A.D., Johanson, U., Braun, T., de Groot, B.L., Fotiadis, D., Kjellbom, P., Engel, A., 2005. The 5A structure of heterologously expressed plant aquaporin SoPIP2;1. J. Mol. Biol. 350, 611–616.

Lefman, J., Morrison, R., Subramaniam, S., 2007. Automated 100-position specimen loader and image acquisition system for transmission electron microscopy. J. Struct. Biol. 158, 318–326.

Mosser, G., 2001. Two-dimensional crystallogenesis of transmembrane proteins. Micron 32, 517–540.

Murata, K., Mitsuoka, K., Hirai, T., Walz, T., Agre, P., Heymann, J.B., Engel, A., Fujiyoshi, Y., 2000. Structural determinants of water permeation through aquaporin-1. Nature 407, 599–605.

Olsen, J.D., Sturgis, J.N., Westerhuis, W.H., Fowler, G.J., Hunter, C.N., Robert, B., 1997. Site-directed modification of the ligands to the bacteriochlorophylls of the light-harvesting LH1 and LH2 complexes of *Rhodobacter sphaeroides*. Biochemistry 36, 12625–12632.

Paul, A., Engelhardt, H., Jakubowski, U., Baumeister, W., 1992. Two-dimensional crystallization of a bacterial surface protein on lipid vesicles under controlled conditions. Biophys. J. 61, 172–188.

Potter, C.S., Pulokas, J., Smith, P., Suloway, C., Carragher, B., 2004. Robotic grid loading system for a transmission electron microscope. J. Struct. Biol. 146, 431–440.

Potter, C.S., Chu, H., Frey, B., Green, C., Kisseberth, N., Madden, T.J., Miller, K.L., Nahrstedt, K., Pulokas, J., Reilein, A., Tcheng, D., Weber, D., Carragher, B., 1999. Leginon: a system for fully automated acquisition of 1000 electron micrographs a day. Ultramicroscopy 77, 153–161.

Rees, D.C., 2001. Crystallographic analyses of hyperthermophilic proteins. Methods Enzymol. 334, 423–437.

Remigy, H.W., Caujolle-Bert, D., Suda, K., Schenk, A., Chami, M., Engel, A., 2003. Membrane protein reconstitution and crystallization by controlled dilution. FEBS Lett. 555, 160–169.

Rigaud, J.L., Mosser, G., Lacapere, J.J., Olofsson, A., Levy, D., Ranck, J.L., 1997. Bio-Beads: an efficient strategy for two-dimensional crystallization of membrane proteins. J. Struct. Biol. 118, 226–235.

Sazinsky, M.H., Mandal, A.K., Arguello, J.M., Rosenzweig, A.C., 2006. Structure of the ATP binding domain from the *Archaeoglobus fulgidus* Cu+ATPase. J. Biol. Chem. 281, 11161–11166.

Scheuring, S., Sturgis, J.N., 2005. Chromatic adaptation of photosynthetic membranes. Science 309, 484–487.

Signorell, G.A., Kaufmann, T.C., Kukulski, W., Engel, A., Remigy, H.W., 2006. Controlled 2D crystallization of membrane proteins using methyl-beta-cyclodextrin. J. Struct. Biol. 157, 321–328.

Stagg, S.M., Lander, G.C., Pulokas, J., Fellmann, D., Cheng, A., Quispe, J.D., Mallick, S.P., Avila, R.M., Carragher, B., Potter, C.S., 2006. Automated cryoEM data acquisition and analysis of 284742 particles of GroEL. J. Struct. Biol. 155, 470–481.

Stevens, T.J., Arkin, I.T., 2000. Do more complex organisms have a greater proportion of membrane proteins in their genomes? Proteins 39, 417–420.

Suloway, C., Pulokas, J., Fellmann, D., Cheng, A., Guerra, F., Quispe, J., Stagg, S., Potter, C.S., Carragher, B., 2005. Automated molecular microscopy: the new Leginon system. J. Struct. Biol. 151, 41–60.

Ubarretxena-Belandia, I., Baldwin, J.M., Schuldiner, S., Tate, C.G., 2003. Three-dimensional structure of the bacterial multidrug transporter EmrE shows it is an asymmetric homodimer. EMBO J. 22, 6175–6181.

Unwin, N., 2005. Refined structure of the nicotinic acetylcholine receptor at 4A resolution. J. Mol. Biol. 346, 967–989.

Urbani, A., Warne, T., 2005. A colorimetric determination for glycosidic and bile salt-based detergents: applications in membrane protein research. Anal. Biochem. 336, 117–124.

Wallin, E., von Heijne, G., 1998. Genome-wide analysis of integral membrane proteins from eubacterial, archaean, and eukaryotic organisms. Protein Sci. 7, 1029–1038.

Walz, T., Jamieson, S.J., Bowers, C.M., Bullough, P.A., Hunter, C.N., 1998. Projection structures of three photosynthetic complexes from *Rhodobacter sphaeroides*: LH2 at 6 A, LH1 and RC-LH1 at 25 A. J. Mol. Biol. 282, 833–845.

Xu, C., Rice, W.J., He, W., Stokes, D.L., 2002. A structural model for the catalytic cycle of Ca(2+)-ATPase. J. Mol. Biol. 316, 201–211.